Atmos. Chem. Phys., 11, 8497–8513, 2011
www.atmos-chem-phys.net/11/8497/2011/
doi:10.5194/acp-11-8497-2011

Atmospheric Chemistry and Physics

Oxidation photochemistry in the Southern Atlantic boundary layer: unexpected deviations of photochemical steady state

Z. Hosaynali Beygi[1], H. Fischer[1], H. D. Harder[1], M. Martinez[1], R. Sander[1], J. Williams[1], D. M. Brookes[2], P. S. Monks[2], and J. Lelieveld[1,3]

[1]Max Planck Institute for Chemistry, Department of Atmospheric Chemistry, Mainz, Germany
[2]University of Leicester, Department of Chemistry, Atmospheric Chemistry Group, UK
[3]The Cyprus Institute, Nicosia, Cyprus

Received: 22 December 2010 – Published in Atmos. Chem. Phys. Discuss.: 2 March 2011
Revised: 11 August 2011 – Accepted: 15 August 2011 – Published: 22 August 2011

Abstract. Ozone (O_3) is a photochemical oxidant, an air pollutant and a greenhouse gas. As the main precursor of the hydroxyl radical (OH) it strongly affects the oxidation power of the atmosphere. The remote marine boundary layer (MBL) is considered an important region in terms of chemical O_3 loss; however surface-based atmospheric observations are sparse and the photochemical processes are not well understood. To investigate the photochemistry under the clean background conditions of the Southern Atlantic Ocean, ship measurements of NO, NO_2, O_3, J_{NO_2}, $J(O^1D)$, HO_2, OH, RO_x and a range of meteorological parameters were carried out. The concentrations of NO and NO_2 measured on board the French research vessel Marion-Dufresne (28° S–57° S, 46° W–34° E) in March 2007, are among the lowest yet observed.

The data is evaluated for consistency with photochemical steady state (PSS) conditions, and the calculations indicate substantial deviations from PSS ($\Phi > 1$). The deviations observed under low NO_x conditions (5–25 pptv) demonstrate a remarkable upward tendency in the Leighton ratio (used to characterize PSS) with increasing NO_x mixing ratio and J_{NO_2} intensity.

It is a paradigm in atmospheric chemistry that OH largely controls the oxidation efficiency of the atmosphere. However, evidence is growing that for unpolluted low-NO_x ($NO + NO_2$) conditions the atmospheric oxidant budget is poorly understood. Nevertheless, for the very cleanest conditions, typical for the remote marine boundary layer, good model agreement with measured OH and HO_2 radicals has been interpreted as accurate understanding of baseline photochemistry. Here we show that such agreement can be deceptive and that a yet unidentified oxidant is needed to explain the photochemical conditions observed at 40°–60° S over the Atlantic Ocean.

Correspondence to: Z. Hosaynali Beygi
(zeinab.beygi@mpic.de)

1 Introduction

The remote MBL occupies about 25 % of the Earth's surface and provides optimal conditions to study baseline photochemical processes (Monks et al., 1998; Penkett et al., 1997). Ozone plays a central role in atmospheric chemistry as the primary precursor of OH radicals through its photodissociation by solar ultraviolet radiation (Levy, 1971). In the troposphere, including the MBL, O_3 is formed though the oxidation of NO into NO_2 (Crutzen et al., 1994; Logan, 1981). The subsequent photodissociation of NO_2 yields ground state oxygen, which combines with molecular oxygen:

$$NO_2 + h\nu \rightarrow NO + O \quad (\lambda < 424\ \text{nm}) \tag{R1}$$

$$O + O_2(+M) \rightarrow O_3(+M) \tag{R2}$$

(M is an air molecule that removes excess energy)

In turn, ozone can regenerate the NO_2, which together with Reactions (R1) and (R2) constitutes a null-cycle:

$$NO + O_3 \rightarrow NO_2 + O_2 \tag{R3}$$

In conditions where NO-to-NO_2 conversion is dominated by Reaction (R3), the overall process can be described by the "Leighton ratio" φ, representing photostationary steady state (PSS), typically achieved within minutes (Leighton, 1961):

$$\varphi = J_{NO_2}[NO_2]/k_3[O_3][NO] \quad (1)$$

J_{NO_2} is the photodissociation frequency of NO_2 and k_3 the rate coefficient of Reaction (R3). In the polluted high-NO_x atmosphere φ is unity (Carpenter et al., 1998; Parrish et al., 1986; Thornton et al., 2002; Yang et al., 2004). In moderately polluted environments radical reactions play a proportionally larger role in the conversion of NO to NO_2 and φ is typically >1 (Hauglustaine et al., 1999; Mannschreck et al., 2004; Ridley et al., 1992; Volz-Thomas et al., 2003). In this case the reactions of peroxy radicals HO_2 and RO_2 with NO compete with Reaction (R3) (R represents an alkyl group, in the clean marine atmosphere mostly CH_3O_2 from CH_4 oxidation) (Crutzen et al., 1994).

In fact by only considering Eq. (1) we are disregarding additional reactions which are expected to be important at low NO_x, i.e. that of NO with HO_2 and RO_2. Thus we need to expand the denominator of Eq. (1) with the following reactions to account for the NO_2 source terms:

$$HO_2 + NO \rightarrow NO_2 + OH \quad (R4)$$

$$RO_2 + NO \rightarrow NO_2 + RO \quad (R5)$$

By rearranging in order to calculate the NO_2 concentration at PSS we obtain:

$$[NO_2]_{calculated} = (k_3[O_3] + k_4[HO_2] + k_5[RO_2])[NO]/J_{NO_2} \quad (2)$$

Several researchers have actually used the measured deviation from $\varphi = 1$ to estimate the concentration of peroxy radicals (Cantrell et al., 1997; Hauglustaine et al., 1999; Parrish et al., 1986; Ridley et al., 1992; Thornton et al., 2002). There is a general disagreement among the theoretically calculated RO_x concentrations and the observed and model calculated RO_x. This is also the case in this study as discussed below.

One cause for such disagreement could be an unknown or non-quantified oxidation pathway which can result in the additional oxidation of NO to NO_2. Since it is unaccounted for in the Leighton ratio this leads to a significant overestimation of the theoretically calculated RO_x compared to measured or model calculated RO_x. One additional pathway leading to deviations of φ=1, relevant for the MBL, is the reaction of NO with halogen monoxides (XO) (Carpenter et al., 1998; Read et al., 2008; Yang et al., 2004). XO (ClO, BrO or IO) can convert NO to NO_2 via the reaction:

$$XO + NO \rightarrow NO_2 + X. \quad (R6)$$

Halogen oxides have been observed in remote marine regions (Yang et al., 2004) and possible XO contribution to the PSS of NO_x and O_3 is discussed in more detail below.

Deviations also occur when loss processes for O_3 other than Reaction (3) become significant, so that O_3 is no longer in steady state. The additional loss processes can be O_3 photolysis, reactions of O_3 with NO_2, alkenes and radicals. At sunrise and sunset deviations are expected from unity due to small J_{NO_2} values, therefore steady state assumptions are not valid.

If the reaction time is not sufficient after perturbations in concentration of gases in the air mass e.g. due to source pollution, then PSS assumption is not valid. The decomposition of reservoir species such as Peroxy Acetyl Nitrate (PAN) as additional NO_2 sources can also result in deviations from PSS. Reaction rates in the Leighton equation are also important for PSS calculations. The calculated ratios are significantly influenced by the uncertainties in the reaction rates of k_1, k_2 and k_3. Uncertainties in the measured values of J_{NO_2}, O_3, NO, NO_2 and RO_x are another important factor. It is vitally important to carry out accurate, precise and simultaneous measurements of the mentioned species in order to better understand the causes for deviations.

Here we present evidence that, indeed, PSS photochemistry is well characterized in polluted conditions, including the MBL. But in the low-NO_x conditions encountered during a ship cruise, sailing between the southern tips of South America and South Africa in the austral summer of 2007, we observed major deviations in φ that cannot be reconciled with the prevalent theory, indicating a major gap in our understanding of baseline atmospheric photochemistry.

2 Experimental

2.1 Cruise MD160

The Marion Dufresne cruise, referred to as MD160, took place during the late austral summer, from 1 March 2007 in Punta Arenas, Chile (70.85° W, 53.12° S), to 23 March 2007 in La Réunion Island (55.36° E, 21.06° S). The cruise was part of the OOMPH project (Ocean Organics Modifying Particles in both hemispheres, see: www.atmosphere.mpg.de/enid/oomph). The ship crossed the southern Atlantic Ocean from west to east between approximately 60° S to 20° S (Fig. 1). In this region of the globe strong westerlies prevail and severe weather and sea conditions are common, as indicated by the terms "Roaring Forties" and "Furious Fifties".

During the first part of the campaign drifting icebergs from Antarctica were often encountered, associated with cold air from the Southern Ocean. During this period cloud cover was extensive with periods of rain and sometimes snow. In contrast, during the second part of the campaign, cruising towards the African continent, both the temperature and radiation levels increased. The westerly wind speeds varied in strength from calm conditions up to 33 m s^{-1}. Occasionally, gale force winds (>17 m s^{-1}) occurred. The average wind speed was 10 m s^{-1} during the first half and 8 m s^{-1} in the second part of the campaign. Further details can be found in (Williams et al., 2010).

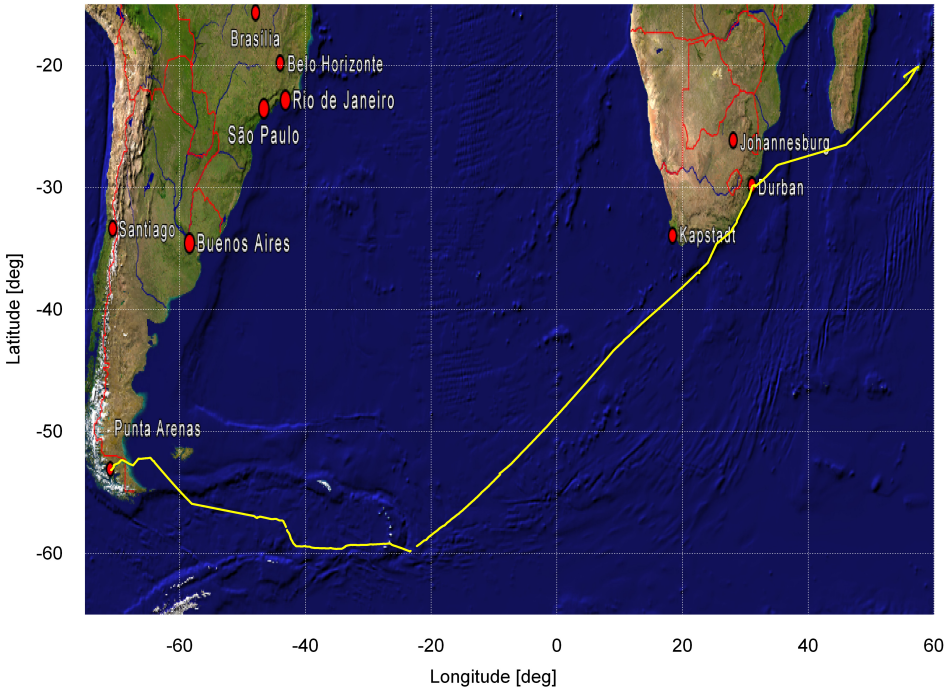

Fig. 1. The Marion Dufresne cruise track over the South Atlantic Ocean.

2.2 Instrumental methods

The most common meteorological measurements were performed, and in addition also balloon soundings, flux measurements and calculations of air flow dynamics and turbulence around the ship. In situ gas phase measurements included O_3, CO, OH, HO_2, RO_x ($RO + RO_2 + HO_x$), NO and NO_2 concentrations as well as organic species like dimethyl sulphide (DMS), isoprene and halocarbons. Measurement of photodissociation frequencies were also performed on board the ship. The NO_x and non-methane hydrocarbon concentrations measured were among the lowest reported to date. During pristine background conditions average ozone mixing ratios were $19.6\,(\pm 0.6)\,ppb_v$ and NO_x mixing ratios $13.4\ (\pm 5.8)\,ppt_v$ ($\pm 1\sigma$ standard deviation). Note that the NO_x data used in the following calculations exclude those that were below the total uncertainty (2σ) of the NO and NO_2 measurements, 1.5 and 2.2 pptv, respectively, though the results and conclusions are robust and consistent by including all data. We focus on the period 13–18 March 2007 during which a complete data set was obtained in air that spent at least 10 days over the Southern and South Atlantic Oceans and Antarctica without contact with air masses near the South American and African continents (Hosaynali Beygi, 2010).

2.2.1 NO_x and O_3 measurements

The instrument used to measure NO_x and O_3 is a high resolution and highly sensitive 3-channel chemiluminescence detector (CLD, ECO-Physics CLD 790 SR) which carries out simultaneous in situ measurements of NO_2, NO and O_3. The instrument was originally manufactured as a two channel system by ECO Physics Inc., Dürnten, Switzerland, and has been modified. One important modification has been the addition of a third channel for the measurement of O_3 (Hosaynali Beygi, 2010).

To guarantee data quality, calibrations were performed during the campaign via the addition of a standard gas directly to the sample lines of the 3 channels. NO in N_2 (2.191 ± 0.044 ppmv, Air Liquide, Germany) was used as a calibration gas. The gas had a flow of 3.93 sccm and was diluted to mixing ratios of approximately $2\,ppb_v$ by synthetic air (SA). This standard was compared to a primary standard (4.83 ± 0.05 ppmv, NIST, USA) before and after the campaign. The NO and NO_2 channels were calibrated at least once per day.

Bottled synthetic air (Air Liquide, Germany), a zero air generator and a Purafil cartridge were employed in order to achieve optimum zeroing conditions for the CLD instrument. The bottled synthetic air used had a purity of 5.0 (corresponding to 99.9990 %) and the air consisted of a mixture of O_2 (20.5 %) and N_2 (the rest) produced by Air Liquide, Germany.

Table 1. Average and standard deviation of zero gas measurements for NO.

Date	Average "zero gas" (pptv)	STDEV "zero gas" (1σ, pptv)
13.03.07	1	1.4
14.03.07	0.8	1.3
15.03.07	0.8	1.3

Table 2. Observed night time NO during pristine background conditions.

Date	Median night time (pptv)	Average night time (pptv)	STDEV night time (pptv)
13.03.07	0.12	0.12	1.31
14.03.07	0.18	0.18	1.32
15.03.07	0.84	1.01	1.67

Since the synthetic air can potentially contain interfering species a zero air generator was used. The zero air generator (CAP 30, Headline Filters GmbH, Germany) consisted of Pd and Pt catalysts and operated at a temperature of 370 °C. It was primarily used to remove hydrocarbons, aerosols and fine dust from bottled air used for zeroing of the instrument. Prior to the campaign the effects of a different variety of Purafil compounds were tested on the quality of the zero air in the laboratory. To avoid Purafil dust contamination, filters were used to prevent contamination of the inlet line and reaction chambers by the Purafil cartridge. The average and standard deviation of zero gas measurements for the NO channel are presented in Table 1. The indicated values have been calculated using the original 2 s data.

The conditions under which the measurements were performed were ideal in terms of testing the zeroing of the instrument. Since measurements were made in a pristine region without direct anthropogenic source pollution, it may be assumed that night time values measured during these periods are based on the complete conversion of NO to NO_2. Due to the lack of solar radiation the back-conversion of NO_2 to NO does not take place and therefore in a remote location without local NO_x sources the NO mixing ratio is expected to equal zero. The standard deviation of the measured night time values was compared to the standard deviation of the SA measurements. They were in very good agreement, which corroborates the high quality (purity) of the synthetic gas (Tables 1 and 2).

The background signal of the three channels was determined with SA measurements and corrected for in the data. The detection limit (DL) of the measured species in this study was determined based on the reproducibility of the SA measurements carried out on a daily basis throughout the campaign. The DL, based on a 2σ confidence level and 60 s integration time, is 0.47 pptv, 0.51 pptv, and 18.2 pptv for the NO, NO_2 and O_3 channels, respectively.

Table 3. Average and standard deviation of zero gas measurements for NO_2.

Date	Average "zero gas" (pptv)	STDEV "zero gas" (1σ, pptv)
13.03.07	10.1	1.7
14.03.07	9.7	1.6
15.03.07	11.4	1.4

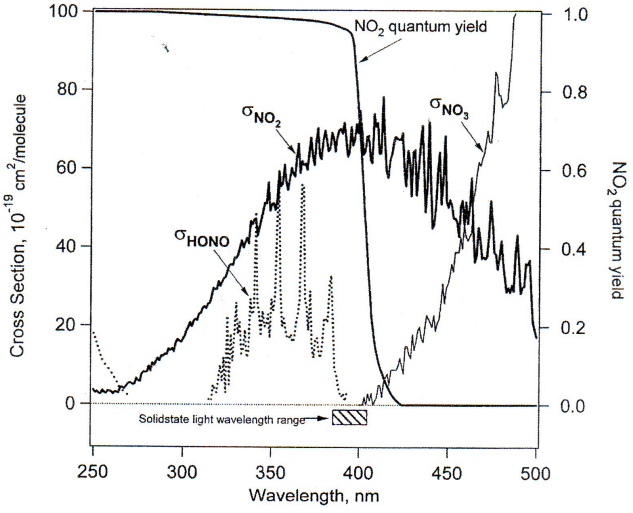

Fig. 2. BLC spectral information. The narrow wavelength range of the solid state LED's avoids effects of interfering species (source: BLC instrument manual, Droplet measurement technologies, USA).

NO_2 was measured using a blue light converter which is a solid state photolytic converter (manufactured by Droplet Measurement Technologies, Colorado, USA). It uses an array of ultraviolet light emitting diodes (UV-LEDs) to photodissociate NO_2 into NO at a wavelength of approximately 395 nm. The LED's are mounted on a BeO (beryllium oxide) substrate and covered with a silicone overcoat. The sample gas passes the photolysis cell and the NO_2 is converted to NO by the UV light from the LEDs. This type of BLC can have a conversion efficiency (CE) of 100 % for 4 s residence time. The conversion efficiency of the BLC depends strongly on the residence time of the air sample in the cell. The residence time is a function of both cell flow and cell pressure. Lower pressure levels result in shorter residence times within the BLC and as a result lead to a decrease in the CE. Therefore, the CE of the BLC is highest at sea level pressure (which

was the case during the campaign). The CE is also affected by the flow rate. High flow rates result in shorter residence times within the BLC and consequently lead to a lower CE. The residence time within the BLC was 1 s.

High specificity is achieved by the narrow spectral output of the LEDs. The peak absorption cross section for NO_2 is at 390–400 nm, i.e. the wavelength range of the LEDs. This precludes the conversion of potential interfering species such as HONO, NO_3 and PAN (Fig. 2). This is discussed in more detail in Sect. 3.3.

The efficiency of the converter has been determined by gas phase titration (GPT) of NO with O_3, before and during the campaign using a commercial instrument (ANSYCO GmbH, Karlsruhe, Germany). The calibration technique is based on the rapid gas phase reaction between NO and O_3 to produce stoichiometric quantities of NO_2. For this purpose both synthetic air and NO calibration gas were used. The quantitative knowledge of this reaction is such that when the NO concentration is known, the concentration of NO_2 can be determined. O_3 is added to NO in a dynamic calibration system, and the NO channel of the CL detector is used as an indicator of changes in NO concentration. A UV lamp is located inside the GPT instrument to generate O_3. Upon addition of O_3, the decrease of NO concentration observed in the calibrated NO channel is equivalent to the concentration of NO_2 produced. From these values the CE of the BLC can be estimated.

As mentioned above, standard GPT, calibrations and zeroing of the instrument were carried out which are considered adequate to calculate the uncertainty and conversion efficiency. The efficiency of the BLC did not change significantly through the course of the campaign. The conversion efficiency during the period of study was 59 % with an uncertainty of ±1.8 %. The average and standard deviation of zero gas measurements for the NO_2 channel are presented in Table 3. There is ∼10 pptv offset during zeroing of the instrument. This offset was not seen once the blue light converter (BLC) was switched off. To correct for this the offset has been subtracted from the measurements; therefore, NO_2 values after correction are approximately 10 pptv lower than the measured signal.

The O_3 channel was calibrated using a commercial O_3 calibrator, (model TE49C, Thermo instruments GmbH, Germany) several times during the campaign. The only gas required for this measurement is SA which is fed directly into the O_3 calibrator. Subsequently, O_3 is produced by the O_3 calibrator based on the specified set points e.g. 0 ppb_v, 10 ppb_v, 20 ppb_v … 100 ppb_v, etc. The value measured by the CLD is read and compared to the actual set point value of the O_3 calibrator.

The precision of the NO, NO_2 and O_3 channels deduced from the sum of the DL and the reproducibility of the in-field calibrations was 0.47 pptv +2.68 % (of total reading) for NO, 0.51 pptv + 2.68 % for NO_2 and 0.02 ppb_v + 1 % for O_3, based on a confidence level of 2σ and 60 s integration time.

The accuracy is calculated based on the total sum of the accuracy of the calibration standards used and also the uncertainty due to the offset corrections. The accuracy for the NO_2 channel additionally contains the uncertainties in the conversion efficiency of the BLC. The accuracy is 1.4 pptv + 2 % for the NO channel, 1.5 pptv + 2 % for the NO_2 channel and 0.5 ppb_v for the O_3 channel.

The total uncertainty of the mixing ratio of a species can be determined by using the error propagation equation

$$(\Delta C)^2 = \left(\frac{\partial C}{\partial E_1}\Delta E_1\right)^2 + \left(\frac{\partial C}{\partial E_2}\Delta E_2\right)^2 + \left(\frac{\partial C}{\partial E_3}\Delta E_3\right)^2 + \ldots \quad (3)$$

E_x represents the different parameters with their uncertainties (ΔE_x). Hence the total uncertainty based on the calculations of precision and accuracy is 1.5 pptv + 3.3 % (of total reading) for the NO channel, 2.2 pptv + 5.3 % for the NO_2 channel and 0.5 pptv + 1 % for the O_3 channel.

The CLD instrument was setup inside a container which was located on the deck of the ship (Fig. 3). Air was sampled through a Teflon inlet line which was mounted on top of the atmospheric mast 10 m above the foredeck and approximately 20–25 m above the sea surface. From there an inlet line was installed to the container. The Teflon inlet line was placed inside black tubing in order to prevent photochemistry taking place in the inlet line. The total length of the inlet line was 17.1 m and consisted of 1/2″ Teflon tubing (outer diameter). The last meter of the inlet line consisted of 1/4″ Teflon tubing.

During the campaign the membrane pump maintained a flow of 19.2 SLM. The instrument preserved a total flow rate of 2.25 SLM by the use of a scroll pump. A peroxide analyzer (Aero-laser AL2021) shared the inlet line with the CLD instrument and applied a flow of 3 SLM. Therefore a total flow of 24.45 SLM was maintained in the inlet line. This corresponds to a retention time of 3.4 s. The data was corrected for the residence time.

Inlet line calibrations and zeroing were carried out using a commercial GPT instrument. The standard GPT procedure is followed once in front of the inlet line and subsequently without the inlet line, directly connected to the instrument. Through a series of steps and comparison of the measured values in the two modes the amount of NO lost in the line can be estimated. For the MD160 campaign it is estimated that NO loss due to residence in the inlet line is less than 2 %. Note that zero gas calibrations with and without the inlet line rule out potential memory effects. There were also concerns regarding the inlet perturbations on NO_2 e.g. PAN decomposition. The amount of NO_2 produced in the inlet line through the reaction of NO with O_3 was calculated for different periods of the study. It was found that the contribution due to this reaction was of the order of 1 % or less of the total NO_2 mixing ratio.

With regard to PAN decomposition, it is important to stress that PAN is relatively stable under the conditions the measurements were carried out, due to the low temperatures,

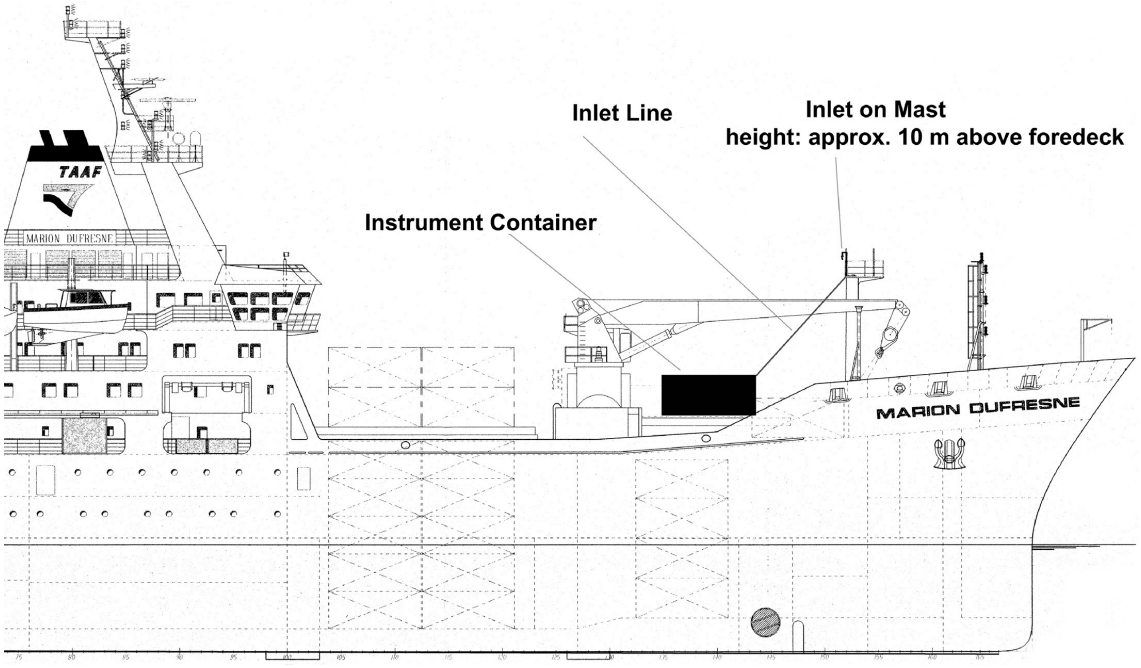

Fig. 3. Schematic of the Marion Dufresne to illustrate the position of the instrument container (black box) relative to the atmospheric mast (Zorn et al., 2008).

which varied on average between 3 °C and 11 °C from 13 to 15 March, respectively. We calculated that PAN under the measurement conditions has an average lifetime of more than 1 day (see Sect. 3.3). We also calculated that in order for PAN to produce 7 pptv of additional NO_2, via thermal decomposition very high concentrations of PAN would be needed, i.e. at least several hundred pptv, which was not observed during the campaign.

2.2.2 Radical and J_{NO_2} measurements

For the data analysis several parameters measured with other instruments were used. The most important details of the instruments are presented next.

OH and HO_2 were measured with the HORUS instrument (HydrOxyl Radical measurement Unit based on fluorescence Spectroscopy), which uses laser-induced fluorescence (LIF) of the OH molecule, based on the fluorescent assay by gas expansion (FAGE) technique. A detailed description of the instrument is given in (Martinez et al., 2010). The time resolution for OH and HO_2 detection is 10 s. The precision for a 60 s integration time and a confidence level of 1σ is 0.017 pptv for OH and 0.1 pptv for HO_2. The accuracy is ± 35 % for a confidence level of 2σ. The DL of the instrument is defined as the 2σ precision, assuming it is limited by the background noise.

The photodissociation rate of NO_2, J_{NO_2}, was measured using two (up- and downward) 2π-steradian (sr) filter radiometers (Meteorologie Consult GmbH, Germany), thus providing 4π-sr photodissociation rates. The instrument has a precision of 5 % for 1 s data and an accuracy of 10 %. The basic design is adopted from the device described by (Junkermann et al., 1989). The principles of J_{NO_2} filter radiometry are explained by (Volz-Thomas et al., 1996). The radiometer is annually calibrated at the research centre FZ-Jülich. Long term calibrations show a small variation (below 2 %, 1σ) during one year.

RO_x was measured using a peroxy radical chemical amplifier (PERCA). The PERCA technique was introduced in the early 1980s (Cantrell et al., 1997) and has been widely used since then (Parker et al., 2009). The detector is calibrated by the addition of NO_2 and the chain length is calibrated by the addition of known concentrations of CH_3O_2. During MD160 the instrument was placed on top of the atmospheric mast above the foredeck. The PERCA instrument is sensitive to humidity hence a water correction is applied to all data. One data point was obtained per minute, however due to calibrations actual measurements are available every other minute. The uncertainty in the PERCA measurements leads to an accuracy of 36 %.

The uncertainty and DL of the relevant instruments used in this work are summarized in Table 4. For each measurement the total uncertainty is determined by the highest of the two values (pptv or %).

Table 4. Total uncertainty of the instrumentation.

Parameter	Instrument	Total uncertainty	Detection limit
NO	CLD	1.5 pptv + 3.3 % ($\pm 2\sigma$ −60 s)	0.47 pptv
NO_2	CLD and BLC	2.2 pptv + 5.3 % ($\pm 2\sigma$ −60 s)	0.51 pptv
O_3	CLD	0.5 ppb_v + 1 % ($\pm 2\sigma$ −60 s)	18.2 pptv
J_{NO_2}	Filter radiometer	11 % (2σ 1 s)	1.5×10^{-6} (s^{-1})
HO_2	LIF instrument	0.1 pptv + 35 % ($\pm 2\sigma$ −10 s)	0.2 pptv
OH	LIF instrument	0.017 pptv + 35 % ($\pm 2\sigma$ −10 s)	0.034 pptv
RO_x	PERCA	10 pptv + 36 % ($\pm 2\sigma$ − 60 s)	10 pptv

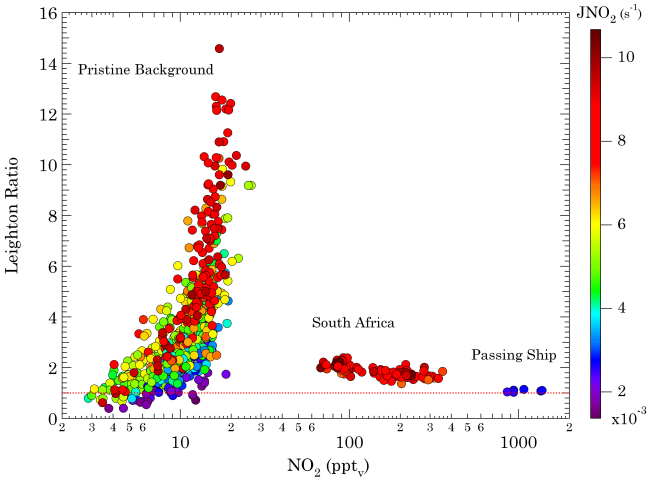

Fig. 4. Leighton ratio calculated from observations in the unpolluted MBL, in moderately polluted air near South Africa, and in the pollution plume of a passing ship. The color coding indicates the NO_2 photodissociation frequency (which scales with light intensity). We estimate the 2σ uncertainty in φ at approximately 93 %, 71 %, 63 % and 11 % for NO_2 mixing ratios of 3, 5, 10 and 100 pptv, respectively.

3 Results and discussions

3.1 Back trajectory calculations and data filtering

Meteorological data and the Lagrangian Analysis Tool (LAGRANTO) were used to calculate the 10-day back trajectories of the air masses (Wernli and Davies, 1997).

Every 3 h about 10 trajectories were started within a 30 min time interval at the ship position along the cruise track. The path of the trajectories was calculated using three-dimensional wind fields from the European Centre for Medium-Range Weather Forecasts (ECMWF). For the analysis, 6-h operational global analyses are complemented by intermediate 3-h forecasts interpolated onto a horizontal grid with a resolution of 1° latitude/longitude. The horizontal resolution of the model is 25 km using 91 vertical levels. The computational time step for trajectory calculations is 30 min.

The 10-day back-trajectories show that the air masses came from the Southern and South Atlantic Ocean until 21st March, and that they originated mostly in the free troposphere, subsiding to the boundary layer before the measurements. Considering the air mass origins over the Antarctic continent and the surrounding oceans, the likelihood of anthropogenic contamination is small.

Depending on the wind direction and speed, the ship exhaust can be a source of contamination. During some periods wind from the rear gave rise to local pollution, which could be easily identified in many of the trace gas measurements. To exclude these events, measurement data with exhaust contamination were removed. The optimum filtering process was selected after considering a range of techniques and criteria. For the data used in PSS calculations additional J_{NO_2} filtering and a filter based on the uncertainty of the channels were applied.

The criteria for data exclusion included the wind direction relative to the direction of the ship, and signs of exhaust contamination in the CLD data. Pollution was observed when the wind came from 55° and 275° relative to the ship (0° is the cruise direction). Further, a rigorous NO filter (based on 2 s measurements) was applied by removing outliers (3σ relative to the 24 h average).

To carry out precise and accurate PSS calculations two additional filters were used. In the remote MBL the NO and NO_2 concentrations are very low and close to the detection limit of the instrument. To ensure data quality a third filter was set up using the total uncertainty based on the calculations of precision and accuracy of the NO and NO_2 channels. Any data point which was below the total uncertainty limit of the relevant channel was excluded. The 2σ uncertainty for the NO and NO_2 channels are 1.5 pptv and 2.2 pptv, respectively. To investigate the influence of this procedure, PSS calculations were carried out both with and without the uncertainty filter. The results of the two sets of calculations did not show significant differences.

Furthermore, PSS calculations are sensitive to uncertainties in J_{NO_2}. At low J_{NO_2} values, e.g. during sunrise and sunset, deviations from PSS are expected. Therefore only data for $J_{NO_2} > 0.001\,s^{-1}$ have been used.

3.2 The Leighton ratio

Figure 4 presents the Leighton ratios based on our observations in the unpolluted MBL. Considerable deviations from unity are evident, as predicted by previous studies

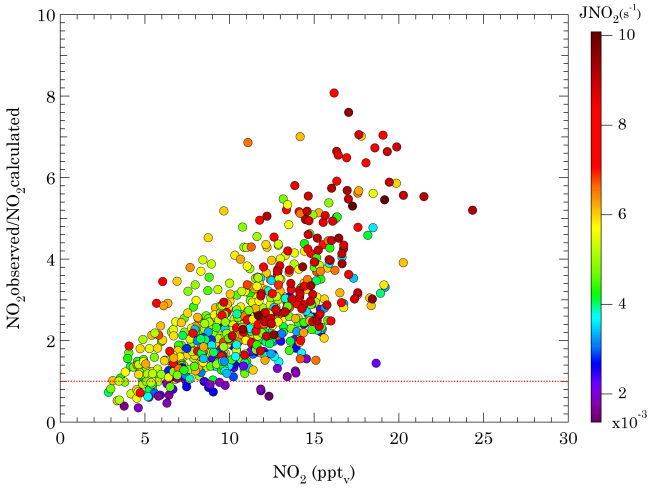

Fig. 5. The ratio of the observed and the PSS-calculated NO_2 concentrations as a function of NO_2 in the unpolluted MBL. The color coding indicates the NO_2 photodissociation frequency.

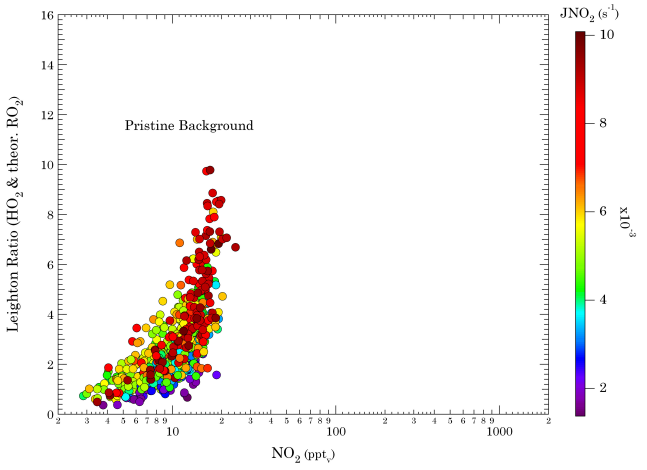

Fig. 6. Leighton ratio calculated using HO_2 and theoretically assumed equal mixing ratio of RO_2, as a function of NO_2 mixing ratios. The colour bar indicates the J_{NO_2} intensity.

(Hauglustaine et al., 1999; Mannschreck et al., 2004; Parrish et al., 1986; Volz-Thomas et al., 2003). However, noteworthy is the trend in φ in the low-NO_x regime, at variance with previous reports, and consistently observed during several days. If RO_2 were a significant contributor to NO-to-NO_2 conversion, it would have been expected that the maximum influence on φ and deviations from unity occur at the lower end of the NO_2 axis, i.e. around 3 pptv, and that the divergence decreases with increasing NO_2. This tendency is actually observed in the moderately polluted air masses near South Africa (70–400 pptv NO_2) and close agreement is found for an air mass that was polluted by a passing ship ($\sim$1 ppb_v) (Fig. 4).

The J_{NO_2} colour coding shows that the maximum deviations are not at the lowest NO_2 and J_{NO_2} values, as expected from the established theory. In fact, for NO_2 mixing ratios less than 10 pptv and J_{NO_2} below $3\text{–}4 \times 10^{-3}\,s^{-1}$ we find that $\varphi \approx 1$ (within the uncertainty range). What is observed is that the maximum deviations in the unpolluted MBL occur at the highest NO_2 mixing ratios (10–20 pptv) and the highest solar radiation intensities (proportional to J_{NO_2}). This clearly indicates the importance of NO_x-mediated photochemistry. Unfortunately no data are available for the 20–60 pptv NO_2 (30–100 pptv NO_x) regime, and we anticipate that a reverse tendency to that for 3–20 pptv NO_2 (5–30 pptv NO_x) may occur and an increasing dominance of Reaction (R3).

Next we analyze to what degree $\varphi \neq 1$ conditions can be explained by conventional theory, in particular by considering measurement uncertainties, and then also by making some assumptions about parameters that were not directly observed. The uncertainty in φ in the low-NO_x regime is mainly related to the NO and NO_2 measurement data.

For NO_x mixing ratios in the pptv range the uncertainty resulting from the measurement of NO and NO_2 dominates the overall uncertainty, which increases with decreasing NO_x. Uncertainty estimates for PSS calculations have been reported to be up to 60 % (Mannschreck et al., 2004). The overall uncertainty in the Leighton ratio φ can be calculated through the sum of the individual uncertainties in each parameter using the following equation:

$$\Delta\varphi = \sqrt{\varphi^2 . \sum \left(\frac{\Delta X_i}{X_i}\right)^2} \quad (4)$$

X_i represents J_{NO_2}, NO, NO_2, HO_2, O_3 and RO_2, depending on which form of the PSS equation is used. For example, for Eq. (1) the uncertainty is calculated as:

$$\Delta\varphi = \sqrt{\varphi^2 . \left(\left(\frac{\Delta JNO_2}{JNO_2}\right)^2 + \left(\frac{\Delta NO_2}{NO_2}\right)^2 + \left(\frac{\Delta k_3}{k_3}\right)^2 + \left(\frac{\Delta O_3}{O_3}\right)^2 + \left(\frac{\Delta NO}{NO}\right)^2\right)} \quad (5)$$

With the addition of parameters to the equation, the uncertainties are added to the total uncertainty. The uncertainties can be expressed as a function of the NO_2 mixing ratios. We estimate the 2σ uncertainty in φ at approximately 93 %, 71 %, 63 % and 11 % for NO_2 mixing ratios of 3, 5, 10 and 100 pptv, respectively.

As mentioned before by only considering Eq. (1), we are disregarding additional reactions which are expected to be important at low NO_x, i.e. that of NO with HO_2 and RO_2. Therefore in a further step Eq. (2) was used in order to calculate the NO_2 concentration at PSS. For this calculation we initially adopt $[HO_2] \approx [RO_2]$, a reasonable assumption for conditions in which hydrocarbon chemistry is dominated by methane (Crutzen et al., 1994), hence $[RO_2] \approx [CH_3O_2]$ (to be evaluated below). Our analysis indicates a 2σ uncertainty of $[NO_2]_{calculated}$ based on Eq. 2) of about 108 %, 89 % and 82 % at NO_2 mixing ratios of 3, 5 and 10 pptv, respectively.

If this expansion of Eq. (1) by including Reactions (R4) and (R5) would adequately account for NO-to-

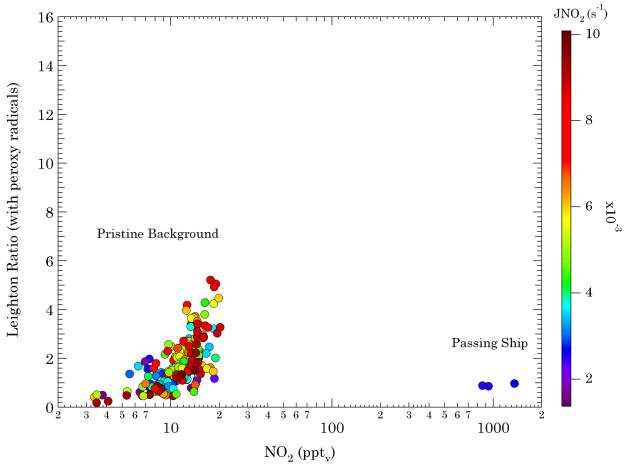

Fig. 7. Leighton ratio calculated using peroxy radical measurements from the PERCA instrument plotted as a function of NO_2 mixing ratios. The colour bar indicates the J_{NO_2} intensity. Total uncertainties were calculated for the Leighton ratio, for several NO_2 mixing ratios and are estimated to be 158 %, 147 % and 131 % for NO_2 mixing ratios of 3, 5 and 10 pptv respectively.

NO_2 conversions, both the adjusted φ and the ratio $[NO_2]_{observed}/[NO_2]_{calculated}$ would be unity. Figure 5 shows that this is clearly not the case and the discrepancy ranges up to a factor of ∼7. We also see that the largest deviations from unity occur in air masses with the highest J_{NO_2}, whereas for low J_{NO_2} the ratio actually approximates unity. Again this is suggestive of a yet unaccounted photochemically driven oxidation process. Note that we have repeated these calculations for moderate-NO_x and high-NO_x conditions for which we obtain good agreement ($[NO_2]_{observed} \approx [NO_2]_{calculated}$).

To investigate the effect of the peroxy radicals, the Leighton ratio was calculated in a second step using measured HO_2 and theoretically assumed RO_2. In this step it is assumed that RO_2 concentrations were similar to those of HO_2 based on model output and previous knowledge (as discussed below). The result of the analysis is demonstrated in Fig. 6. A decrease can be seen in the deviations from unity; however it is clear that the addition of peroxy radicals can not explain the deviations. In a third step to further investigate the effect of peroxy radicals on the Leighton ratio, calculations were carried out using peroxy radical mixing ratios obtained from the PERCA instrument instead of the theoretically assumed RO_2 data. The results of this calculation are presented in Fig. 7. In this case a dramatic change is observed in the Leighton ratio of the pristine background conditions. That is, the maximum deviation seen in Fig. 7 is substantially lower compared with the values in Figs. 4 and 6.

The trend seen in the deviation from φ=1 as a function of NO_2 and J_{NO_2} in the pristine background air masses does not change. In fact it is the same as for the classic Leighton ratio. This may again be an indication for an unknown photochemically driven oxidant that can convert NO to NO_2 and therefore leads to significant deviation from unity in the Leighton ratio.

The values for the passing ship period have not changed and are similar to those plotted in Fig. 4. This is a strong confirmation of the relative insignificance of RO_x reactions in high NO_x regimes.

Total uncertainties were calculated for the Leighton ratio, for several NO_2 mixing ratios and are estimated to be 158 %, 147 % and 131 % for NO_2 mixing ratios of 3, 5 and 10 pptv respectively. The uncertainties are higher than in previous cases due to the additional uncertainties in the peroxy instrument.

It is remarkable that the addition of PERCA derived peroxy radical concentrations causes such a strong change in the Leighton ratio and can to a large degree compensate for the high NO_2 concentrations measured by the CLD instrument. Figure 8 presents time series of observed J_{NO_2} and radical species in addition to NO_x and O_3. Maximum OH mixing ratios reach up to ∼0.3 pptv, HO_2 ∼17 pptv and RO_x ∼150 pptv. As the mixing ratios of the highly reactive OH and RO are low it may be assumed that their contribution to RO_x is minor. As a consequence maximum RO_2 mixing ratios would exceed 100 pptv, clearly inconsistent with the above assumption that $RO_2 \approx HO_2$.

This assumption can be tested with a chemical box model, constrained by our measurements, and with output of a global chemistry-transport model.

A photochemical steady-state box model was used to simulate the ambient HO_x, OH and CH_3O_2 concentrations ($RO_2 \approx CH_3O_2$). The model was set up and constrained using data obtained on the MD 160 cruise. The parameters used to constrain the box model are: H_2, CH_4, H_2O_2, CH_3OOH, O_3, NO, CO, latitude, longitude, pressure, air temperature, H_2O, JO^1D, J_{NO_2}, and a number of photolysis rates based on radiation calculations using measured J_{NO_2} as input, JCHOH, $JCOH_2$, JH_2O_2, JCH_3OOH and JNO_3. Steady state concentrations of OH, HO_2 and CH_3O_2 were calculated according to the method of (Kubistin et al., 2010). A model data point was calculated whenever the complete set of relevant data was available within a 10 s time period.

Under steady state conditions the production and loss rates for the radical species balance:

$$\frac{d[X]}{dt} \approx 0 = P_x - L_x \quad (6)$$

where P_x represents the total production and Lx the loss rate. By this approach the diurnal profiles of the radicals and their average concentrations could be reproduced well, as shown in Fig. 9. Figure 10 demonstrates that according to these calculations HO_2 and CH_3O_2 concentrations are very similar. This is in line with the observed CO/CH_4 ratio, as expected according to the prevailing theory of atmospheric radical photochemistry, because the production of HO_2 and

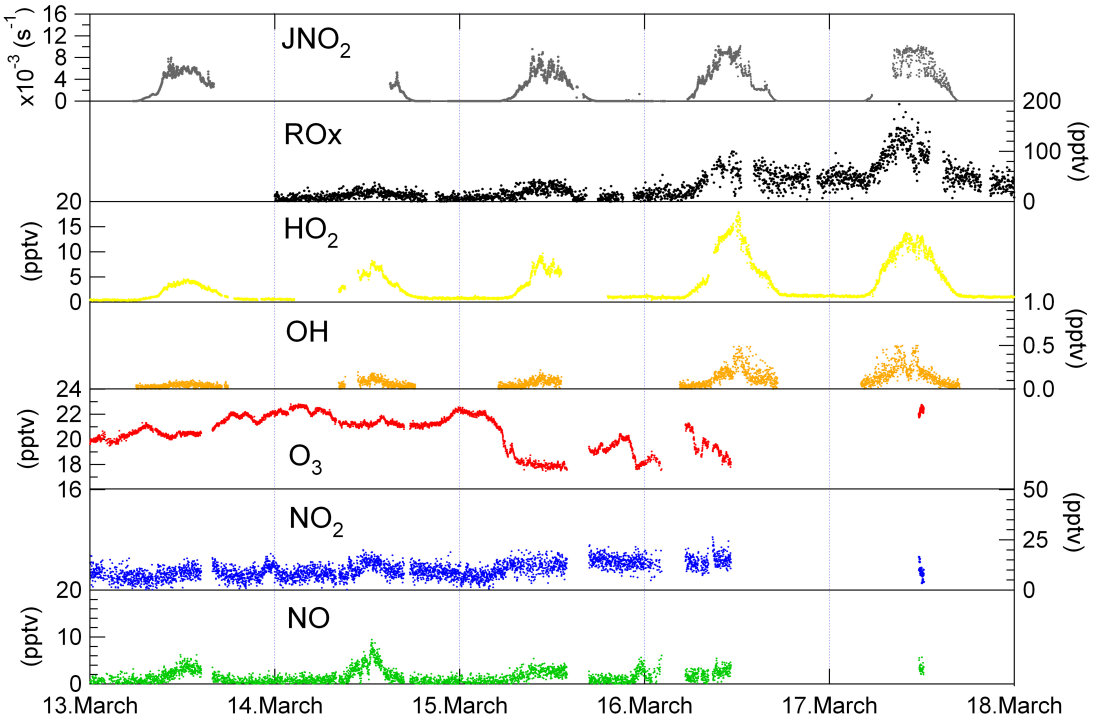

Fig. 8. Measured diurnal profiles of NO, NO_2, O_3, J_{NO_2}, OH, HO_2 and RO_x (note that NO_x and O_3 data have been filtered for stack emissions).

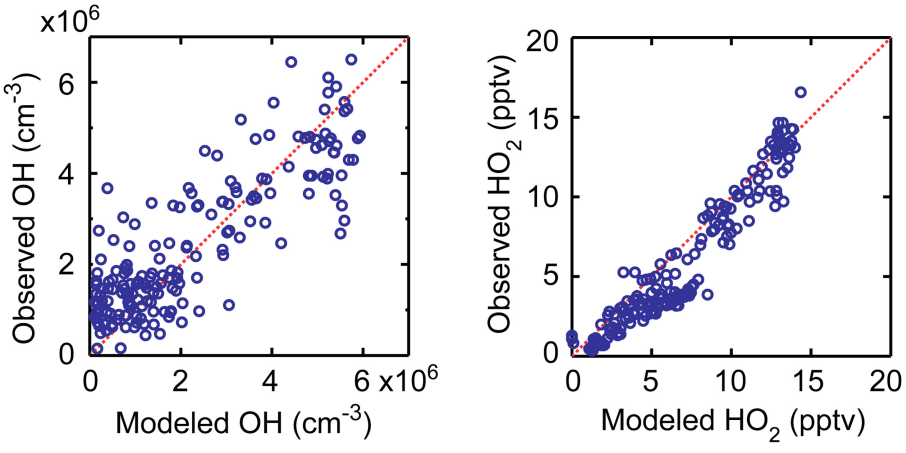

Fig. 9. Comparison of model results with observations of OH and HO_2 (for NO < 20 pptv).

CH_3O_2 are dominated by the reactions of CO and CH_4 with OH, respectively.

A further test of the assumption of $HO_2 \approx CH_3O_2 \approx RO_2$ is based on calculations with an atmospheric chemistry general circulation model (AC-GCM). The ECHAM/MESSy Atmospheric Chemistry (EMAC) model describes lower and middle atmosphere processes and their interactions with oceans, land and human influences (Jöckel et al., 2010; Kerkweg et al., 2008). The dynamical core atmospheric general circulation model is the 5th generation European Centre Hamburg model ECHAM5 (Roeckner et al., 2006).

EMAC was applied in the T42L90-resolution, i.e. with a spherical truncation of T42 (corresponding to about $2.8° \times 2.8°$ latitude/longitude) with 90 vertical hybrid pressure levels up to 0.01 hPa. The model time step in this resolution is 12 min. Data from the model were sampled at each time step along the OOMPH transect. The results corroborate that for the clean background period until 17 March 2007

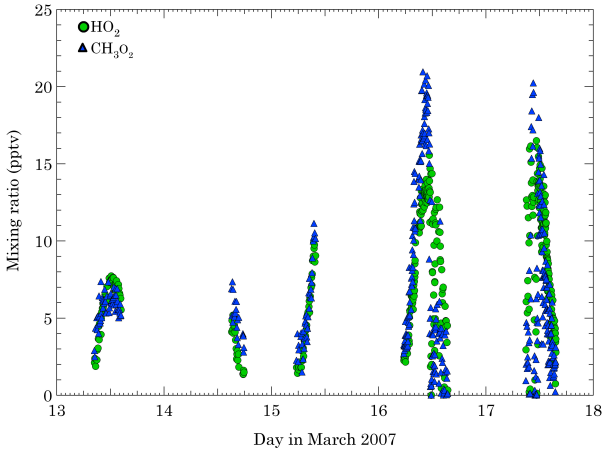

Fig. 10. Results from the chemical box model for daytime HO_2 and CH_3O_2, obtained by constraining the model with the measurements of non-radical species.

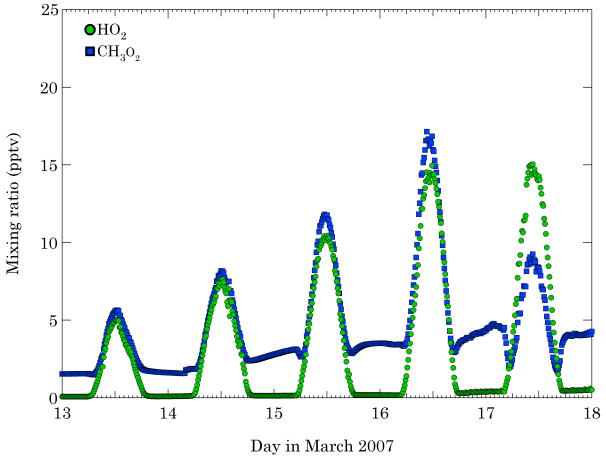

Fig. 11. Results from the global EMAC model for HO_2 and CH_3O_2. The model grid cells correspond with the locations and time periods of the measurements and the results shown in Fig. 10.

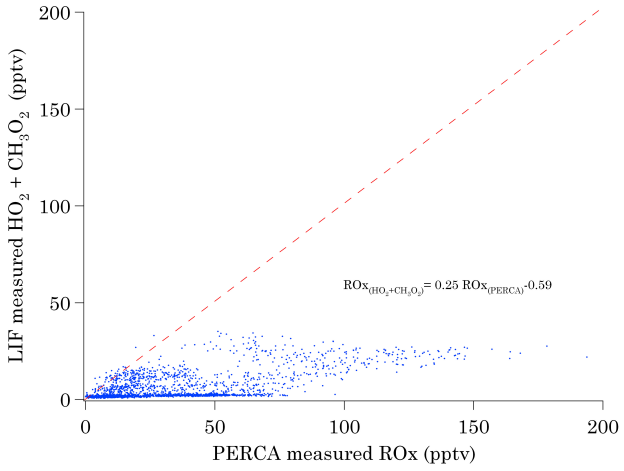

Fig. 12. PERCA measured RO_x vs. RO_x based on LIF measured HO_2 and an estimate of CH_3O_2 (assuming RO_2=CH_3O_2 and that $CH_3O_2 \sim HO_2$). The red dashed line illustrates the 1:1 line.

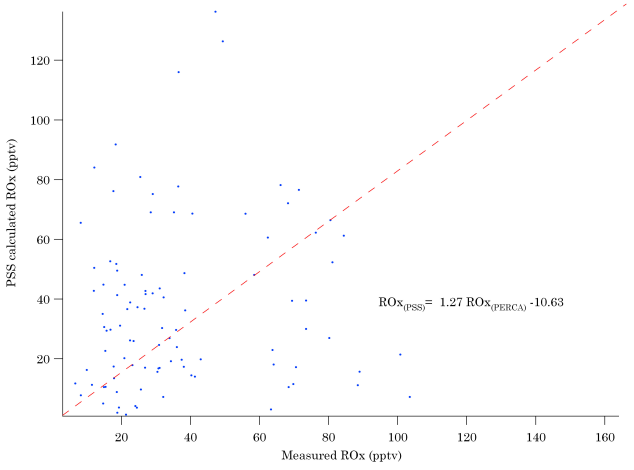

Fig. 13. PERCA measured RO_x vs. PSS calculated RO_x. The red dashed line illustrates the 1:1 line.

(EMAC predicts somewhat enhanced pollution influences thereafter, related to its coarse resolution), during daylight hours RO_2 and HO_2 concentrations are about equal (Fig. 11). A closer look at the RO_2 specie as predicted by EMAC, i.e. CH_3O_2, $C_2H_5O_2$, $C_3H_7O_2$ and $C_4H_9O_2$, reveals that CH_3O_2 is in fact the dominant RO_2 specie and that the mixing ratios of the other species compared to CH_3O_2 are negligible. Therefore based on EMAC predictions we can assume that $RO_2 \approx CH_3O_2$. As mentioned above, based on previous knowledge this is a reasonable assumption for conditions in which hydrocarbon chemistry is dominated by methane.

The results from both the box model and EMAC corroborate the expectation that $RO_2 \approx CH_3O_2 \approx HO_2$. Therefore this assumption is valid based on current knowledge of the MBL chemistry and represented by state-of-the-art models. The realistic representation of HO_x by our constrained box model, in agreement with the global model, is supported by the favourable comparison between the model output and measurements (Fig. 9). However at the same time a significant inconsistency results from the comparison of model calculated and measured RO_x data. A number of studies have been carried out in which measurements of peroxy radicals have been compared with PSS-based calculations and model results, typically under moderately polluted (>50 pptv NO_x) or highly polluted conditions (up to several ppb_v NO_x) (Cantrell et al., 1997; Carpenter et al., 1998; Hauglustaine et al., 1999; Ridley et al., 1992; Volz-Thomas et al., 2003). Generally, RO_2 concentrations calculated by the PSS assumption were significantly higher than the directly measured values. It is remarkable that both our

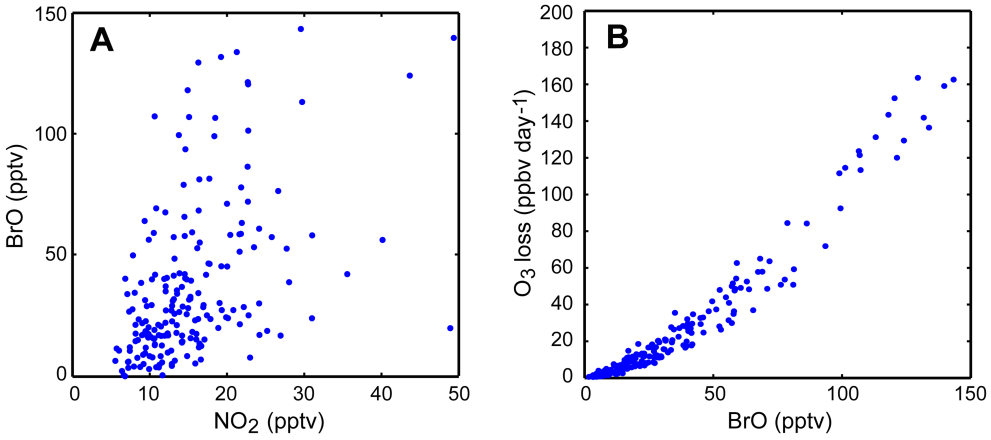

Fig. 14. Results from the chemical box model, constrained by the measurements, assuming a Leighton ratio of $\varphi = 1$.

PSS-derived and observed RO_x are much higher than those predicted by the models and based on previous knowledge, which is demonstrated in Figs. 12 and 13, which show a scatter plot of RO_x based on LIF measured HO_2 and an estimate of CH_3O_2 (assuming RO_2=CH_3O_2 and that $CH_3O_2 \sim HO_2$) and PSS derived RO_x versus measured RO_x, respectively. Figure 12 nicely demonstrates that our understanding of the radical chemistry in the MBL based on our current understanding and also based on box models and 3-D model results accounts for less than 20 % of the measured "peroxy" radicals. The equation is $RO_{x(HO_2+CH_3O_2)} = 0.25\ RO_{x(PERCA)} - 0.59$. The slope we see in the plot is as anticipated with an R^2 value of 0.64. Figure 13 confirms that the atmosphere (PSS) and the PERCA see similar results, i.e. similar amounts of "peroxy" radicals or more generally peroxy radicals plus a mystery oxidizer that converts NO to NO_2 and undergoes amplification in the PERCA. The equation in this case is $RO_{x(PSS)} = 1.27\ RO_{x(PERCA)} - 10.63$. Although the data scatter around the 1:1 line, the correlation coefficient is rather poor.

This difference can be interpreted in two ways. First there may be systematic errors involved in measuring and calculating RO_x and RO_2. Second there is an unknown photochemical oxidant that converts NO into NO_2. The process apparently maintains the OH/HO_2 relationship, as indicated by Fig. 9; and the effects vanish as NO_x increases. The fact that the RO_x mixing ratios are so high suggests that the PERCA instrument is also sensitive to the unknown oxidant (to be discussed below). Actually, the RO_x measurements provide independent observational support of an unknown oxidant that causes the anomalous Leighton ratios.

3.3 BLC and potential interfering species

The peak absorption cross section for NO_2 is at 390–400 nm, i.e. the wavelength range of the LEDs. This precludes the conversion of potential interfering species such as HONO, NO_3 and PAN (Fig. 2).

Furthermore, based on the very low PAN concentrations calculated by our atmospheric chemistry general circulation model (EMAC, discussed in article) and PAN measurements during the campaign, which were below the DL of the instrument (10 pptv), potential interferences from this species are highly unlikely, as several hundred pptv would be required to cause significant effects through thermal decomposition. Also due to the relatively low temperatures during the cruise, the lifetime of PAN was calculated to be about 1.2 days, indicating that it is thermally stable under the measurement conditions.

To investigate which species could cause possible interferences in the BLC, the absorption cross sections (ACS) of many species were studied and compared to the ACS of NO_2 for three different wavelengths, i.e. 390, 395 and 400 nm (source: the MPI-Mainz spectral atlas at http://www.atmosphere.mpg.de/enid/2295). Species which have been suggested as potentially interfering are PAN, nitrous and nitric acid (HONO and HNO_3), alkyl nitrates (e.g. methyl nitrate and ethyl nitrate), and halogen nitrates ($BrONO_2$, $ClONO_2$, ClNO, $ClNO_2$ and $BrNO_2$). The results of this study are summarized in Table 5.

The NO_2 equivalent of each species needed to produce 7 pptv of additional NO_2 was calculated and is listed in Table 5. A dash in the table means that there is no corresponding ACS for the species in the wavelength of interest.

From Table 5 it can be concluded that these species may not be expected to cause significant interferences in the BLC. $BrNO_2$ is the only specie with an ACS close enough to that of NO_2 at the wavelength of interest. However calculation of the mixing ratio of $BrNO_2$ needed to produce 7 pptv of NO_2 shows that on average 26 pptv would be required, which we consider highly unlikely in view of the model calculations presented in the article.

Table 5. Absorption cross section of potentially interfering species.

	ASC at 390 nm	ASC at 395 nm	ASC at 400 nm	NO_2 equivalent (7 pptv)
NO_2	5.90×10^{-19}	6.10×10^{-19}	6.50×10^{-19}	–
$BrONO_2$	2.90×10^{-20}	2.60×10^{-20}	2.30×10^{-20}	142
$ClONO_2$	9.10×10^{-22}	7.60×10^{-22}	6.40×10^{-22}	4538
ClNO	6.86×10^{-20}	5.97×10^{-20}	5.13×10^{-20}	60
$ClNO_2$	4.75×10^{-21}	–	3.27×10^{-21}	869
$BrNO_2$	1.60×10^{-19}	1.50×10^{-19}	1.40×10^{-19}	26
HONO	2.40×10^{-20}	6.00×10^{-21}	–	172
PAN	–	–	–	–
HNO_3	–	–	–	–
Methyl nitrate	–	–	–	–
Ethyl nitrate	–	–	–	–

3.4 PERCA method and potential interferences

The most widely used method to measure RO_x is based on the Peroxy Radical by Chemical Amplification (PERCA) technique (Cantrell et al., 1993; Penkett et al., 1997). NO is added to the air mixture containing RO_2 and HO_2, yielding NO_2, which can be detected by several methods. The PERCA method was also employed in our measurement campaign (Fleming et al., 2006). An inherent problem is that oxidants in addition to RO_2/HO_2 that convert NO into NO_2 are detected ambiguously. For example, it has been shown that halogen oxides (ClO), especially in the presence of CO, catalytically oxidize NO. The measurement principle of the PERCA method is based on the OH/HO_2 radical catalysed simultaneous chain oxidation of CO to CO_2 and NO to NO_2:

$$HO_2 + NO \rightarrow NO_2 + OH \quad \text{(R7)}$$

$$OH + CO \rightarrow CO_2 + H \quad \text{(R8)}$$

$$H + O_2 + M \rightarrow HO_2 + M \quad \text{(R9)}$$

RO_2 measurement first requires the conversion of RO_2 to HO_2 via the following reactions:

$$RO_2 + NO \rightarrow NO_2 + RO \quad \text{(R10)}$$

$$RO + O_2 \rightarrow RCHO + HO_2 \quad \text{(R11)}$$

$$\rightarrow \text{R-CO-R} + HO_2 \quad \text{(R12)}$$

Subsequently HO_2 is detected through the same cycle as the first three reactions mentioned above. Therefore any oxidant that converts NO to NO_2 and has a sufficiently long chain length (i.e. the number of conversion cycles that occurs before termination) can be detected via the chemical amplification method. In a study by (Perner et al., 1999) it was observed that the method is sensitive to ClO_x (Cl+ClO+ClO_2). It was found that ClO_x is reduced by NO to Cl atoms which react with CO in the presence of O_2:

$$ClO + NO \rightarrow Cl + NO_2 \quad \text{(R13)}$$

$$Cl + CO + M \rightarrow ClCO + M \quad \text{(R14)}$$

The reaction sequence which is initiated oxidizes CO to CO_2 and NO to NO_2:

$$ClCO + O_2 + M \rightarrow ClCO_3 + M \quad \text{(R15)}$$

$$ClCO_3 + NO \rightarrow Cl + CO_2 + NO_2 \quad \text{(R16)}$$

The chain length for ClO_x species in the study by Perner et al. was reported to be 300 ± 60. In parallel peroxy radicals are indicated with a chain length of 160 ± 15. Therefore the chain length for ClO_x is approximately a factor of two larger than that of the peroxy radicals. It is actually possible that the ClO_x chain length could be up to a factor of 10 higher compared to the peroxy radical chain length (J. N. Crowley, personal communication, 2009). This would of course have a significant impact on the total observed "RO_x signal". Thus the chemical amplification method is not specific and does not indicate which radical chain is observed. Therefore the PERCA signal can be defined as:

$$\text{PERCA signal} = RO_2 + RO + HO_2 + OH + X \quad (7)$$

X in the above equation is the additional unknown oxidant that can oxidize NO to NO_2 in the atmosphere and therefore lead to the high NO_2 levels measured during the campaign.

The possibility that unidentified NO-to-NO_2 conversions have affected our PERCA measurements actually reconciles the above two interpretations. The unexpected high RO_x mixing ratios as measured with the PERCA instrument, being up to an order of magnitude higher than of measured HO_2 and of modelled HO_2 and RO_2 provides independent observational support for the presence of an unknown oxidant. Furthermore, its production is likely to be catalytic as it produces a strong signal in the PERCA instrument.

3.5 Halogen monoxides, DMS and the Leighton ratio

Several researchers have proposed that halogen monoxides can represent an "unknown oxidant" and drive φ away from unity, although their studies did not pertain to baseline MBL chemistry (Mannschreck et al., 2004; Matsumoto et al., 2006). Further, Read et al. (2008) conclude that biologically active regions of the tropical Atlantic Ocean release reactive halogens (up to 2.5 pptv BrO) and destroy ozone. This contrasts with our measurements in a region of very low biological activity. The part of the numerator in Eq. (2) between parentheses would have to be expanded by another term k_6[XO], with X representing e.g. bromine. Both our chemical box and global chemistry-transport models include comprehensive descriptions of halogen chemistry in the MBL. Our model calculations indicate only very low concentrations of BrO in the measurement region (well below 1 pptv), one reason being that in the remote MBL the sea salt aerosol is hardly acidified by strong acids (e.g. H_2SO_4) of natural and anthropogenic origin. Back-calculating from Eq. (2), assuming that $[NO_2]_{observed}/[NO_2]_{calculated}$ is unity, implies that a BrO mixing ratio up to ~100 pptv would be required. This would represent a "bromine explosion" leading to the depletion of O_3 and NO_x, which is not observed.

We have used the chemical box model, which includes a comprehensive description of halogen chemistry (Kerkweg et al., 2008) to investigate the potential role of bromine in the observed deviation of the Leighton ratio. We constrained the model with the observations and applied an artificial emission of Br_2 from the sea salt aerosol (or a surface source) and increased the entrainment of ozone from the free troposphere to prevent its complete chemical destruction. For a Leighton ratio ϕ=1 the simulated mixing ratio of BrO ranges from a few to more than 100 pptv at low to high solar intensity, respectively (Fig. 14a). These BrO mixing ratios are orders of magnitude higher than those simulated with a three-dimensional global model (Kerkweg et al., 2008). If the marine boundary layer chemistry would sustain such high BrO mixing ratios, it would be extremely difficult to explain the observed O_3 levels of ~20 ppb_v. Figure 14b shows that 10–30 pptv BrO, for example, destroys 5–15 ppb_v O_3 during the day, which would give rise to a strong diurnal cycle of O_3 in the boundary layer, which is not observed. Although we do not exclude that halogen chemistry takes place, it seems highly unlikely that reactive bromine accounts for the "mystery" oxidant.

The contribution of DMS has been considered as a potential source of peroxy radicals as this compound was measured during the campaign. However, the ship sailed across regions with very low biological activity at the time of the measurements, and mixing ratios of DMS, and other volatile organic compounds (VOCs) such as isoprene, were rather low, i.e. DMS averaged about 50 pptv, which is too low to have a significant effect.

3.6 Uncertainty related to rate coefficients

The uncertainty related to the rate coefficients of relevant reactions, k_i, is of course part of the overall uncertainty of the PSS calculations. It is believed that whilst k_i does in fact contribute to the overall uncertainty of the results, there is little dispute over the actual k_i values themselves. This was noticed in the sensitivity tests carried out on the PSS calculations using two studies of rate coefficients (e.g., Atkinson et al., 2004; Sander et al., 2006).

The two rate coefficients agree well within the range of uncertainty. Therefore it is concluded that the large deviations seen in the Leighton ratios cannot be due to the relatively insignificant uncertainty in the k_i values.

The assumption that the reaction rate coefficients of RO_2 with NO are similar to that of HO_2 has been commonly used in the past. However, it has been suggested that the reaction rate coefficients of RO_2 and HO_2 could be critical for PSS calculations of RO_x (Matsumoto et al., 2006). Therefore a sensitivity test was carried out in relation to rate coefficients, in this case specifically for RO_x calculated from the PSS expression ($[RO_x]_{PSS}$). It was found that the reaction rates of NO with HO_2 and RO_2 are critical for the PSS estimation and that $[RO_x]_{PSS}$ can be influenced by uncertainties in the rate coefficients. Therefore it is recommended that the above assumption should be practiced with caution.

4 Conclusions

Our measurements provide compelling evidence of the presence of an unknown oxidant. It might only convert NO into NO_2, but also has the potential of participating in catalytic oxidant cycles, as indicated by the PERCA measurements. Note that even though the uncertainties increase with decreasing NO_2, at the very lowest levels of 3–5 pptv φ approaches one (Fig. 4), which argues against a measurement error to explain the exponentially increasing φ-values at NO_2 mixing ratios up to 20 pptv. Although it is widely accepted that the oxidation chemistry of the troposphere is dominated by reactions with OH (Crutzen et al., 1994; Heard and Pilling, 2003; Logan et al., 1981), a growing number of studies exposes discrepancies between model calculations and observations in low-NO_x conditions (Brune et al., 1998; Faloona et al., 2000; Hofzumahaus et al., 2009; Lelieveld et al., 2008; Stevens et al., 1997; Thornton et al., 2002). It is noteworthy that models and measurements of HO_x in the remote MBL generally agree well, which has been optimistically interpreted as a consistent understanding of baseline photochemistry (Heard and Pilling, 2003; Sommariva et al., 2004). However, taking all indications into account rather suggests that something important is missing in our understanding of baseline photochemistry.

Appendix A

Abbreviations and acronyms

ACS	Absorption cross sections
BLC	Blue light converter
CE	Conversion efficiency
CH_3O_2	Methyl peroxy radical
CLD	Chemiluminescence detector
DL	Detection limit
DMS	dimethyl sulfide
ECHAM	European Centre Hamburg general circulation model
EMAC	ECHAM/MESSy Atmospheric chemistry model
GPT	Gas phase titration
HO_2	Hydroperoxy radical
J_{NO_2}	Photolysis rate of NO_2
LED	Light emitting diodes
LIDAR	Laser detection and ranging
LIF	Laser induced fluorescence
MBL	Marine boundary layer
MD	Marion Dufresne
MESSy	Modular earth sub-model system
MPI	Max Planck Institute
NO	Nitrogen oxide
NO_2	Nitrogen dioxide
NO_x	Total sum of active nitrogen oxides ($NO+NO_2$)
OH	Hydroxyl radical
OOMPH	Organics over Ocean Modifying Particles in both hemispheres
PAN	Peroxy acetyl nitrate
PERCA	Peroxy radical chemical amplifier
ppb_v	parts per billion
pptv	parts per trillion
PSS	Photostationary state
RO_2	Organic peroxy radical
RO_x	Total sum of organic peroxy radicals
SA	Synthetic air
Sccm	Standard cubic centimetres per minute
SLM	Standard liter per minute
STDEV	Standard deviation
UV	Ultraviolet
VOC	Volatile organic compound

Supplementary material related to this article is available online at: http://www.atmos-chem-phys.net/11/8497/2011/acp-11-8497-2011-supplement.pdf.

Acknowledgements. We are grateful to the OOMPH campaign (MD160) team members: U. Parchatka, C. Gurk, R. Königstedt, S. Wong-Zehnpfennig, S. Zorn, T. Custer, V. Sinha, V. Gros, D. Kubistin and M. Rudolf. We thank the Modular Earth Submodel System (MESSy) team for model support, in particular P. Jöckel. We also thank H. Wernli for providing back trajectory data, and J. Crowley for comments on the manuscript. The authors are grateful for logistical support from the IPEV during the Southern Ocean cruise. The OOMPH project was funded under the EU sixth framework program (018419).

The service charges for this open access publication have been covered by the Max Planck Society.

Edited by: R. Ebinghaus

References

Atkinson, R., Baulch, D. L., Cox, R. A., Crowley, J. N., Hampson, R. F., Hynes, R. G., Jenkin, M. E., Rossi, M. J., and Troe, J.: Evaluated kinetic and photochemical data for atmospheric chemistry: Volume I – gas phase reactions of O_x, HO_x, NO_x and SO_x species, Atmos. Chem. Phys., 4, 1461–1738, doi:10.5194/acp-4-1461-2004, 2004.

Brune, W. H., Faloona, I. C., Tan, D., Weinheimer, A. J., Campos, T., Ridley, B. A., Vay, S. A., Collins, J. E., Sachse, G. W., Jaegle, L., and Jacob, D. J.: Airborne in-situ OH and HO_2 observations in the cloud-free troposphere and lower stratosphere during SUCCESS, Geophys. Res. Lett., 25, 1701–1704, 1998.

Cantrell, C. A., Shetter, R. E., Lind, J. A., McDaniel, A. H., Calvert, J. G., Parrish, D. D., Fehsenfeld, F. C., Buhr, M. P., and Trainer, M.: An Improved Chemical Amplifier Technique for Peroxy Radical Measurements, J. Geophys. Res.-Atmos., 98, 2897–2909, 1993.

Cantrell, C. A., Shetter, R. E., Calvert, J. G., Eisele, F. L., Williams, E., Baumann, K., Brune, W. H., Stevens, P. S. and Mather, J. H.: Peroxy radicals from photostationary state deviations and steady state calculations during the tropospheric OH photochemistry experiment at Idaho Hill, Colorado, 1993, J. Geophys. Res.-Atmos., 102, 6369–6378, 1997.

Carpenter, L. J., Clemitshaw, K. C., Burgess, R. A., Penkett, S. A., Cape, J. N. and McFadyen, G. C.: Investigation and evaluation of the NO_x/O_3 photochemical steady state, Atmos. Environ., 32, 3353–3365, 1998.

Crutzen, P. J., Lelieveld, J., and Bruehl, C.: Advances in Environmental Science and Technology, Wiley, New York, 1994.

Faloona, I., Tan, D., Brune, W. H., Jaegle, L., Jacob, D. J., Kondo, Y., Koike, M., Chatfield, R., Pueschel, R., Ferry, G., Sachse, G., Vay, S., Anderson, B., Hannon, J., and Fuelberg, H.: Observations of HO_x and its relationship with NO_x in the upper troposphere during SONEX, J. Geophys. Res.-Atmos., 105, 3771–3783, 2000.

Fleming, Z. L., Monks, P. S., Rickard, A. R., Bandy, B. J., Brough, N., Green, T. J., Reeves, C. E., and Penkett, S. A.: Seasonal dependence of peroxy radical concentrations at a Northern hemisphere marine boundary layer site during summer and winter: evidence for radical activity in winter, Atmos. Chem. Phys., 6, 5415–5433, doi:10.5194/acp-6-5415-2006, 2006.

Hauglustaine, D. A., Madronich, S., Ridley, B. A., Flocke, S. J., Cantrell, C. A., Eisele, F. L., Shetter, R. E., Tanner, D. J., Ginoux, P., and Atlas, E. L.: Photochemistry and budget of ozone during the Mauna Loa Observatory Photochemistry Experiment

(MLOPEX 2), J. Geophys. Res.-Atmos., 104, 30275–30307, 1999.

Heard, D. E. and Pilling, M.J.: Measurement of OH and HO_2 in the troposphere, Chem. Rev., 103, 5163–5198, 2003.

Hofzumahaus, A., Rohrer, F., Lu, K. D., Bohn, B., Brauers, T., Chang, C. C., Fuchs, H., Holland, F., Kita, K., Kondo, Y., Li, X., Lou, S. R., Shao, M., Zeng, L. M., Wahner, A., and Zhang, Y. H.: Amplified Trace Gas Removal in the Troposphere, Science, 324, 1702–1704, 2009.

Hosaynali Beygi, Z.: Oxidation photochemistry in the remote marine boundary layer, PhD Thesis, International Max Planck Research School, Johannes Gutenberg University Mainz, Germany, 2010.

Jöckel, P., Kerkweg, A., Pozzer, A., Sander, R., Tost, H., Riede, H., Baumgaertner, A., Gromov, S., and Kern, B.: Development cycle 2 of the Modular Earth Submodel System (MESSy2), Geosci. Model Dev., 3, 717–752, doi:10.5194/gmd-3-717-2010, 2010.

Junkermann, W., Platt, U., and Volz Thomas, A.: A photoelectric detector for the measurement of photolysis frequencies of Ozone and other atmospheric molecules, J. Atmos. Chem., 8, 203–227, 1989.

Kerkweg, A., Jöckel, P., Warwick, N., Gebhardt, S., Brenninkmeijer, C. A. M., and Lelieveld, J.: Consistent simulation of bromine chemistry from the marine boundary layer to the stratosphere – Part 2: Bromocarbons, Atmos. Chem. Phys., 8, 5919–5939, doi:10.5194/acp-8-5919-2008, 2008.

Kubistin, D., Harder, H., Martinez, M., Rudolf, M., Sander, R., Bozem, H., Eerdekens, G., Fischer, H., Gurk, C., Klpfel, T., Königstedt, R., Parchatka, U., Schiller, C. L., Stickler, A., Taraborrelli, D., Williams, J., and Lelieveld, J.: Hydroxyl radicals in the tropical troposphere over the Suriname rainforest: comparison of measurements with the box model MECCA, Atmos. Chem. Phys., 10, 9705–9728, doi:10.5194/acp-10-9705-2010, 2010.

Leighton, P. A.: Photochemistry of air pollution, Phys. Chem., 9, 300 pp., 1961.

Lelieveld, J., Butler, T. M., Crowley, J. N., Dillon, T. J., Fischer, H., Ganzeveld, L., Harder, H., Lawrence, M. G., Martinez, M., Taraborrelli, D., and Williams, J.: Atmospheric oxidation capacity sustained by a tropical forest, Nature, 452, 737–740, 2008.

Levy, H.: Normal Atmosphere – Large Radical and Formaldehyde Concentrations Predicted, Science, 173, 141–143, 1971.

Logan, J. A.: Tropospheric chemistry a global perspective, Am. Chem. Soc., 86, 7210–7254, 1981.

Mannschreck, K., Gilge, S., Plass-Duelmer, C., Fricke, W., and Berresheim, H.: Assessment of the applicability of NO-NO_2-O_3 photostationary state to long-term measurements at the Hohenpeissenberg GAW Station, Germany, Atmos. Chem. Phys., 4, 1265–1277, doi:10.5194/acp-4-1265-2004, 2004.

Martinez, M., Harder, H., Kubistin, D., Rudolf, M., Bozem, H., Eerdekens, G., Fischer, H., Klpfel, T., Gurk, C., Königstedt, R., Parchatka, U., Schiller, C. L., Stickler, A., Williams, J., and Lelieveld, J.: Hydroxyl radicals in the tropical troposphere over the Suriname rainforest: airborne measurements, Atmos. Chem. Phys., 10, 3759–3773, doi:10.5194/acp-10-3759-2010, 2010.

Matsumoto, J., Kosugi, N., Nishiyama, A., Isozaki, R., Sadanaga, Y., Kato, S., Bandow, H., and Kajii, Y.: Examination on photostationary state of NO_x in the urban atmosphere in Japan, Atmos. Environ., 40, 3230–3239, 2006.

Monks, P., Carpenter, L. J., Penkett, S. A., Ayers, G. P., Gillett, R. W., Galbally, I. E., and Meyer, C. P.: Fundamental ozone photochemistry in the remote marine boundary layer: the soapex experiment, measurement and theory, Atmos. Environ., 32, 3647–3664, 1998.

Parker, A. E., Monks, P. S., Wyche, K. P., Balzani-Lööv, J. M., Staehelin, J., Reimann, S., Legreid, G., Vollmer, M. K., and Steinbacher, M.: Peroxy radicals in the summer free troposphere: seasonality and potential for heterogeneous loss, Atmos. Chem. Phys., 9, 1989–2006, doi:10.5194/acp-9-1989-2009, 2009.

Parrish, D. D., Trainer, M., Williams, E. J., Fahey, D. W., Hubler, G., Eubank, C. S., Liu, S. C., Murphy, P. C., Albritton, D. L., and Fehsenfeld, F. C.: Measurements of the NO_x-O_3 Photostationary State at Niwot Ridge, Colorado, J. Geophys. Res.-Atmos., 91, 5361–5370, 1986.

Penkett, S. A., Monks, P. S., Carpenter, L. J., Clemitshaw, K. C., Ayers, G. P., Gillett, R. W., Galbally, I. E., and Meyer, C. P.: Relationships between ozone photolysis rates and peroxy radical concentrations in clean marine air over the Southern Ocean, J. Geophys. Res.-Atmos., 102, 12805–12817, 1997.

Perner, D., Arnold, T., Crowley, J., Klupfel, T., Martinez, M., and Seuwen, R.: The measurement of active chlorine in the atmosphere by chemical amplification, J. Atmos. Chem., 34, 9–20, 1999.

Read, K. A., Mahajan, A. S., Carpenter, L. J., Evans, M. J., Faria, B. V. E., Heard, D. E., Hopkins, J. R., Lee, J. D., Moller, S. J., Lewis, A. C., Mendes, L., McQuaid, J. B., Oetjen, H., Saiz-Lopez, A., Pilling, M. J., and Plane, J. M. C.: Extensive halogen-mediated ozone destruction over the tropical Atlantic Ocean, Nature, 453, 1232–1235, 2008.

Ridley, B. A., Madronich, S., Chatfield, R. B., Walega, J. G., Shetter, R. E., Carroll, M. A., and Montzka, D. D.: Measurements and model simulations of the photostationary state during the Mauna-Loa-Observatory photochemistry experiment – Implications for radical concentrations and Ozone production and loss rates, J. Geophys. Res.-Atmos., 97, 10375–10388, 1992.

Roeckner, E., Brokopf, R., Esch, M., Giorgetta, M., Hagemann, S., Kornblüh, Manzini, L. E., Schlese, U., and Schulzweida, U.: Sensitivity of simulated climate to horizontal and vertical resolution in the ECHAM5 atmosphere model, J. Climate, 19, 3771–3791, 2006.

Sander, S. P., Golden, D. M., Kurylo, M. J., Moortgat, G. K., Wine, P. H., Ravishankara, A. R., Kolb, C. E., Molina, M. J., Finlayson-Pitts, B. J., Huie, R. E., and Orkin, V. L.: Chemical Kinetics and photochemical data for use in stratospheric modeling – evaluation number 15, Jet Propulsion Laboratory, California Institute of Technology, California, 2006

Sommariva, R., Haggerstone, A.-L., Carpenter, L. J., Carslaw, N., Creasey, D. J., Heard, D. E., Lee, J. D., Lewis, A. C., Pilling, M. J., and Zdor, J.: OH and HO_2 chemistry in clean marine air during SOAPEX-2, Atmos. Chem. Phys., 4, 839–856, doi:10.5194/acp-4-839-2004, 2004.

Stevens, P. S., Mather, J. H., Brune, W. H., Eisele, F., Tanner, D., Jefferson, A., Cantrell, C., Shetter, R., Sewall, S., Fried, A., Henry, B., Williams, E., Baumann, K., Goldan, P., and Kuster, W.: HO_2/OH and RO(2)/HO_2 ratios during the Tropospheric OH Photochemistry Experiment: Measurement and theory, J. Geophys. Res.-Atmos., 102, 6379–6391, 1997.

Thornton, J. A., Wooldridge, P. J., Cohen, R. C., Martinez, M., Harder, H., Brune,W. H.,Williams, E. J., Roberts, J. M., Fehsenfeld, F. C., Hall, S. R., Shetter, R. E., Wert, B. P., and Fried, A.: Ozone production rates as a function of NOx abundances and HOx production rates in the Nashville urban plume, J. Geophys.Res., 107, D12, doi:10.1029/2001JD000932, 2002.

Volz-Thomas, A., Lerner, A., Patz, H. W., Schultz, M., McKenna, D. S., Schmitt, R., Madronich, S., and Roth, E. P.: Airborne measurements of the photolysis frequency of NO_2, J. Geophys. Res.-Atmos., 101, 18613–18627, 1996.

Volz-Thomas, A., Geiss, H., Hofzumahaus, A., and Becker, K. H.: Introduction to special section: Photochemistry experiment in BERLIOZ, J. Geophys. Res.-Atmos., 108, 8252, doi:10.1029/2001JD002029, 2003

Wernli, H. and Davies, H. C.: A Lagrangian-based analysis of extratropical cyclones. I: The method and some applications, Q. J. Roy. Meteorol. Soc., 123, 467–489, 1997.

Williams, J., Custer, T., Riede, H., Sander, R., Jöckel, P., Hoor,P., Pozzer, A., Wong-Zehnpfennig, S., Hosaynali Beygi, Z., Fischer, H., Gros, V., Colomb, A., Bonsang, B., Yassaa, N., Peeken, I., Atlas, E. L., Waluda, C. M., van Aardenne, J. A., and Lelieveld, J.: Assessing the effect of marine isoprene and ship emissions on ozone, using modelling and measurements from the South Atlantic Ocean, Environ. Chem., 7, 171–182, 2010.

Yang, J., Honrath, R. E., Peterson, M. C., Parrish, D. D., and Warshawsky, M.: Photostationary state deviation-estimated peroxy radicals and their implications for HO_x and ozone photochemistry at a remote northern Atlantic coastal site, J. Geophys. Res. Atmos., 109, D02312, doi:10.1029/2003JD003983, 2004.

Zorn, S. R., Drewnick, F., Schott, M., Hoffmann, T., and Borrmann, S.: Characterization of the South Atlantic marine boundary layer aerosol using an aerodyne aerosol mass spectrometer, Atmos. Chem. Phys., 8, 4711–4728, doi:10.5194/acp-8-4711-2008, 2008.